Vol. 22, No. 1(2023) Alim3003
Revista Mexicana de Ingeniería Química

Rheological and structural properties of complex coacervates of *Amaranthus hypochondriacus* protein-citrus pectin

Propiedades reológicas y estructurales de complejos coacervados de proteína de *Amaranthus hypochondriacus*-pectina cítrica

K. García-de la Rosa[1], C. Lobato-Calleros[2], L. Hernández-Rodríguez[2*], E. Aguirre-Mandujano[2]
[1]*Posgrado en Ciencia y Tecnología Agroalimentaria, Departamento de Ingeniería Agroindustrial, Universidad Autónoma Chapingo, Km. 38.5 Carretera México-Texcoco, 56230 Texcoco, México.*
[2]*Departamento de Preparatoria Agrícola, Universidad Autónoma Chapingo, Km. 38.5 Carretera México-Texcoco, 56230 Texcoco, México.*
Received: November 11, 2022; Accepted: January 11, 2023

Abstract
Complex coacervates were formed by electrostatic interaction between amaranth protein isolated (API) and citrus pectin (CP), at different API:CP weight ratio (3:1, 5:1, and 7: 1) and pH values (3.5 and 4.5). Physicochemical, rheological, and microstructural properties of the coacervates were explored. FTIR spectrum of the coacervates showed changes in the peaks at 1636 and 1153 cm^{-1} compared to the spectrum of API and CP, confirming complex coacervates formation. A fine, structured and compact structure was observed in the coacervates made at pH 3.5; in contrast, a matrix composed of relatively large aggregates was observed for the coacervates created at pH 4.5. Coacervates particle size increased as the pH and API:CP weight ratio increased, with the hydrodynamic diameter (D_h) ranging from 1043 ± 39 to 2670 ± 30 nm. The apparent viscosity of the coacervates increased as the API:CP weight ratio increased and pH decreased. All the variations of complex coacervates presented higher values of storage modulus (G') than loss modulus values (G"), suggesting a predominantly elastic rheological conduct. The knowledge generated could contribute to the implementation of the studied coacervates in industrial food processing.
Keywords: Amaranth protein, citrus pectin, complex coacervates, rheology, structure.

Resumen
Se formaron complejos coacervados por interacción electrostática entre aislado de proteína de amaranto (API) y pectina cítrica (CP) a diferentes relaciones de peso API:CP (3:1, 5:1 y 7:1) y pH (3.5 y 4.5). Se investigaron las propiedades fisicoquímicas, reológicas y microestructurales de los coacervados. El espectro FTIR de los coacervados mostró cambios en los picos 1636 y 1153 cm^{-1} en comparación con los espectros de API y CP, lo que confirmó la formación de los coacervados. Se observó una estructura fina y compacta en los coacervados formados a pH 3.5; en cambio, en los formados a pH 4.5 se observó una matriz con agregados relativamente grandes. El tamaño de partícula de los coacervados aumentó al incrementar el pH y la relación en peso API:CP, variando el diámetro hidrodinámico (D_h) de 1043 ± 39 a 2670 ± 30 nm. La viscosidad aparente de los coacervados aumentó a medida que incrementó la relación en peso API:CP y disminuyó el pH. Todas las variaciones de coacervados presentaron valores más altos en el módulo de almacenamiento (G') que en el módulo de pérdida (G"), mostrando un comportamiento reológico predominantemente elástico. El conocimiento generado sobre los coacervados podría contribuir a su implementación en la industria alimentaria.
Palabras clave: Proteína de amaranto, pectina cítrica, complejos coacervados, reología, estructura.

* *Corresponding author. E-mail*: landy14hr@yahoo.com.mx
https://doi.org/10.24275/rmiq/Alim3003
ISSN:1665-2738, *issn-e*: 2395-8472

1 Introduction

Proteins not only constitute food macronutrients and play an essential nutritional role for human beings, but they also exhibit functional properties that make them essential ingredients in many processed foods and affect the final quality of the product (Peña-Solis *et al*., 2023). A disadvantage is that proteins have low stability against environmental stresses, like freezing, pH, heat and pressure (Monroy-Rodríguez *et al*., 2021), but by forming protein complexes with other biopolymers such as polysaccharides its stability is improved. Incorporation of proteins and polysaccharides into food systems contributes to its structure by forming particles and complexes, showing better results in their functional properties (i.e. emulsifier, foaming, structuring, and gelling capacities among others) than individually (Liu *et al*., 2015; Ru *et al*., 2012).

Protein-polysaccharide complexes formation can be carried out by coacervation, which is defined as the division into two aqueous phases of a colloidal dispersion, obtaining a phase with biopolymers and another serum phase in equilibrium (Bosnea *et al*., 2017). Complex coacervation involves electrostatic attractive interactions between oppositely charged biopolymers, being the structure, functional properties and stability of the complexes made affected by pH variations, ionic strength, functional groups, hydrophobicity, protein-polysaccharide weight ratio, total biopolymer concentration, molar ratio, mechanical stress, temperature, surface charge density of proteins, charge density, and rigidity of the polysaccharide (Muriel *et al*., 2020). The study of complex coacervates has focused mainly on those obtained from animal origin proteins, such as fish gelatin, gelatin (Anvari and Chung, 2016; Ifeduba and Akoh, 2016), whey protein, β-lactoglobulin, α-lactalbumin (Ach *et al*., 2015; Comert *et al*., 2016), sodium caseinate (Koupantsis *et al*., 2014) and ovalbumin (Souza and Garcia-Rojas, 2015). However, it should be considered that proteins of animal origin have been related to digestive intolerance or food allergies, even though they are of high biological quality. On the other hand, proteins of vegetable origin are considered an alternative to those of animal origin due to their high bioavailability and low production cost (Motta *et al*., 2019). Nevertheless, few studies have been carried out on proteins of vegetable origin for the formation of coacervates, some of them being soybean, chia, pea, canola, and flaxseed (Chen *et al*., 2020; Guo *et al*., 2020; Hasanvand and Rafe, 2019; Moschakis and Biliaderis, 2017).

In this sense, it is interesting to explore the formation and characterization of coacervates from amaranth protein, which has an adequate balance of essential amino acids and high bioavailability, conferring it with a high nutritional value. This pseudocereal contains between 15 and 17 % of protein made up of prolamin (11 %), albumin (65 %), glutelin (7 %), globulin (17 %), and gliadin (0.01 %), which makes it suitable for its use in producing "gluten-free" food for people with celiac disease (Motta *et al*., 2019). The relevance of the study about the generation and coacervates properties lies in its vast application potential; for example, in the production of edible films, as an encapsulating or trapping material for the delivery of bioactive compounds such as probiotics, vitamins, antioxidants, colorants, and oily solutions (Lan *et al*., 2020). The usefulness of coacervates has also been demonstrated as fat substitutes, stabilizers, emulsifiers, gelling agents, and viscosity modifiers in food matrices for the production of functional products (Niu *et al*., 2018). Thus, the aim of this work was to stablish the conditions to form API-CP complex coacervates, and to evaluate the physicochemical, rheological, and microstructural properties of the complex coacervates as function of the API:CP weight ratio and pH of formation. It is hoped that this knowledge will result in the use of this novel protein-polysaccharide complex as an ingredient for developing functional foods with increased overall performance.

2 Materials and methods

2.1 Materials

Amaranthus hypochondriacus L. variety Revancha seeds were sourced from a local producer in San José Atlán, Huichapan, Hidalgo, Mexico, with GPS coordinates of 20° 20’ 26.4192" N, 99° 41’ 39.7356" W and an elevation of 2150 masl. The seeds were processed to obtain amaranth flour by subsequent defatting and protein isolation.

CEDROSA® citrus pectin with an esterification degree of 74.2 % (Central de Drogas S.A. de C.V., Naucalpan, State of Mexico, Mexico) was used to form protein-polysaccharide complex coacervates. Hexane was supplied by MEYER® (Chemical Reagents, Tlahuac, Mexico City). Sodium hydroxide (NaOH) and hydrochloric acid (HCl) were purchased from J.T. Baker (Xalostoc, State of Mexico, Mexico). In the experiments, deionized (DDW) and distilled water were applied.

2.2 Methods

2.2.1 Obtaining protein isolate from amaranth

API was extracted using to the method defined by Martínez and Añón (1996), making slight modifications. Amaranth seeds were ground for obtaining flour, which was defatted by extraction using a Soxhlet equipment with hexane for 5 h at 75 °C. The defatted flour was left in a laminar flow hood (RDM, LF-102P, Midland, Ontario, Canada) for 4 h with air extraction for total hexane evaporation, and saved in hermetically stamped polyethylene bags at 4 ± 1 °C for later use. Four treatments were established varying the pH values of protein solubilization (9 and 11) and the

precipitation pH values (4 and 5), and coded as: API_{9-5}, API_{11-5}, API_{9-4}, and API_{11-4}. Defatted amaranth flour (10 % w/v) dispersions in DDW (100 g) were prepared, stirred (600 rpm, 60 min) at room temperature (22 ± 2 °C). Subsequently, pH of the solutions was adjusted to 9 or 11 with 1N NaOH depending on the treatment (pH 120, Conductronic, Santa Cruz Buenavista, Puebla, Mexico) and left under continuous stirring for 60 min. Afterwards, the dispersions were centrifuged (Centrifuge 5810 R, Eppendorf, AG, Hamburg, Germany) for 15 min at 9000 × g, maintaining a temperature of 10 °C. pH value of the supernatant was modified to pH 4 or 5 with 1N HCl, depending on the treatment. The precipitated protein was separated by centrifugation at 9000 × g for 15 min at 4 °C. The precipitate was rinsed twice in DDW, adjusted to neutral pH (pH 7) using 0.1N NaOH, then was oven dried (HCF-62, Riossa Digital, Mexico City, Mexico) for 48 h at 40 °C. Dried isolate was ground in a mortar, then saved in hermetically stamped polyethylene bags at 4 ± 1 °C until use. Protein isolate (API_{11-4}) with the highest yield (7.30 ± 0.14 %) was used to form complex coacervates and subjected to determinations of moisture (7.5 ± 0.02 %), ash (3.69 ± 0.07 %), protein (85.06 ± 0.02 %), fat (0.18 ± 0.00 %), and fiber (1.0 ± 0.13 %) (AOAC, 1996).

2.2.2 Zeta potential (ζ-potential) of biopolymers and complex coacervates

The ζ-potential of the API, CP aqueous dispersions (0.01 % w/v, pH 3 to 7), and API-$CP_{a/b}$ (0.01 % w/v, pH 3.5 or 4.5) was measured with a Zetasizer Nano (ZS, Malvern Instruments, Ltd., Malvern, Worcestershire, UK). 0.1N NaOH or 0.1N HCl was used to modify the pH value of the dispersions to the indicated values. From the variation of the ζ-potential values of API and CP as function of the pH, two values of pH (3.5 and 4.5) were selected to prepare de complex coacervates as discussed in section 3.1 (Hernández-Marín *et al*., 2013).

2.2.3 Biopolymer stock solution preparation

Stock solutions of API (3, 5, and 7 % w/w) and CP (1 % w/w) in DDW were placed under slight agitation (600 rpm; RO 15 power, IKA® Werke, Staufen, Germany) during 2 h and 12 h, respectively at room temperature (22 ± 2 °C). The solutions were kept at 4 ± 1 °C for 24 h to permit full hydration.

2.2.4 Elaboration of the complex coacervates

In order, to obtain a general picture for the complexation phenomena and the properties of the complex coacervates formed between API and CP, the impact of three weight ratios between API and CP (3:1, 5:1, and 7:1) at a determined pH value was evaluated (Ramírez-Santiago *et al*., 2012). API dispersions (15 g; 3, 5, and 7 % w/w) were aggregated to CP solution (15 g; 1 % w/w), modifying the pH to 3.5 or 4.5, with 0.1N HCl. The samples were stored for 48 h maintaining a temperature of 4 ± 1 °C, guaranteeing the formation of complex coacervates. Subsequently, to separate the complex coacervates, the samples were centrifuged at room temperature (22 ± 2 °C) for 15 min at 121 × g. The latter were coded as API-$CP_{a/b}$, where “a" represents the weight ratio between API and CP (3:1, 5:1 and 7:1) and “b" the precipitation pH value (3.5 or 4.5) (Hernández-Rodríguez *et al*., 2014).

2.2.5 Protein, moisture content and yield

The protein content of API-$CP_{a/b}$ was estimated using the Kjeldahl method taking into consideration a conversion factor of 6.25 and reported on dry basis. Moisture content was determined with the oven drying method (AOAC, 1995). Coacervation yield was calculated with the following expression:

$$\% CY = \frac{wC}{wTB} \times 100 \quad (1)$$

Where: % CY = coacervate yield; wC = weight of coacervate on a dry basis; wTB = total weight of biopolymers used on a dry basis.

2.2.6 Fourier Transform Infrared Spectroscopy (FTIR)

The infrared spectra of API-$CP_{a/b}$ were determined according to Martínez-Velasco *et al*. (2018), using a spectrophotometer with a universal attenuated total reflectance device (CARY 630 FTIR, Agilent Technologies, Inc., Agilent, CA, USA). Dried samples of API, CP and API-$CP_{a/b}$ (10 mg) were placed on the diamond crystal adjusting the geometry 60 units of force gauge. A range of 4000 - 750 cm^{-1} was used to determine the absorbance, using a spectral resolution of 4 cm^{-1}. 64 scans of each sample were performed and mean values were obtained.

2.2.7 Rheological properties

The rheological behavior of API-$CP_{a/b}$ was established by dynamic (flow curve) and oscillatory (amplitude sweeps) tests in a Physica MCR 301 rheometer (Anton Paar, Messtechnik, Stuttgart, Germany), equipped with a Physica TEK 150P temperature measurement and control system used to maintain the temperature at 4 °C during measurements. A cone-plate geometry of 1° and 50 mm diameter was used. The API-$CP_{a/b}$ (~1.5 g) was placed on the plate and the structure was allowed to recover for 30 min, and a humidification chamber was used to avoid the sample evaporation (Estrada-Girón *et al*., 2014). The flow curves of the API-$CP_{a/b}$ were obtained at a shear rate sweep from 10^{-3} to 10^{3} s^{-1}, recording apparent viscosity values. Software on the equipment fitted the data to the Ellis model (Equation 2), which describes the time-independent behavior of fluids. A frequency of 1 Hz and a strain range in the amplitude sweeps from 0.01 to 100 % were

used to characterize the linear viscoelastic region (LVR) (Hernández-Rodríguez *et al*., 2014).

$$\eta = \frac{\eta_0}{[1 + (\lambda\dot{\gamma})^2]^p} \quad (2)$$

Where: η = apparent viscosity; η_0 = viscosity at low shear rate; λ = relaxation time of biopolymers in solution; $\dot{\gamma}$ = shear rate, and p = shear behavior index.

2.2.8 *Particle size and microstructure*

The mean D_h of the complex coacervates was obtained with a Zetasizer Nano (ZS, Malvern Instruments, Ltd., Malvern, Worcestershire, UK) by measuring dynamic light scattering. The API-CP$_{a/b}$ were diluted to a concentration of 0.01 % w/w in DDW, the pH was modified with 0.1N NaOH or 0.1N HCl to 3.5 or 4.5 depending on the pH value used to form the complex coacervate, was used a potentiometer (pH 120, Conductronic, Santa Cruz Buenavista, Puebla, Mexico); the refractive index of the samples was 1.333 (Hernández-Rodriguez *et al*., 2014).

To observe the API-CP$_{a/b}$ microstructure, a standard technique was used. The samples (~0.1 g) were colored with crystal violet and subsequently observed at 10× magnification in a light microscope (Olympus BX53F, Olympus Optical Corp., Tokyo, Japan) with a Moticam 2500 camera (Motic Incorporation Ltd., Hong Kong, China) and using a Motic Images Plus 2.0 software (Motic, Corp., Ltd., China).

2.2.9 *Statistical analysis*

A completely randomized design of three independent experiments was used, performing all measurements three times. Data were submitted to variance analysis, when it was appropriate to an analysis using the Tukey test. Significance was established at $p \leq 0.05$. Statgraphics 7 software (Statistical Graphics Corp., Manugistics Inc., Cambridge, MA, USA) was used for data analysis.

3 Results and discussion

3.1 *ζ-potential measurements*

The ζ-potential provides the net surface charge of a particle, as well as being an important factor in determining the grade of interaction (repulsion or attraction) between colloidal particles and influences the functional properties of colloidal protein isolates (solubility and emulsifier ability) (Tiwari and Singh, 2012). The ζ-potential values of the API solutions ranged from +18.67 ± 0.25 mV at pH 3 to -30.27 ± 0.38 mV at pH 7 (Figure 1). Ventureira *et al*. (2012) reported similar values, obtaining ζ-potential values for *Amaranthus hypochondriacus* protein isolate from +25 mV (pH 2.0) to -30 mV (pH 8.0).

The surface charge on proteins results from the ionization of surface groups (Shevkani *et al*., 2014); where positive values of the ζ-potential are caused by the protonation of amino group (-NH_2) producing ammonium ions (-NH_3^+); while the negative charges are presented by the ionization of the carboxyl functional group (-COOH) forming carboxylate ions (-COO^-) (Trujillo-Ramírez *et al*., 2018). The zero value of the ζ-potential of API was observed at pH 4.0 (pI), being within the range (pH 4 - 6) reported for amaranth proteins (Bolontrade *et al*., 2013).

The CP presented negative values of ζ-potential in the entire pH range considered, varying from -13.67 ± 0.32 mV at pH 3 to -40.63 ± 0.76 mV at pH 7 (Figure 1). Our results agree with the ζ-potential values informed by Salminen and Weiss (2013) for CP, which varied from -10 mV (pH 3) to -41.5 mV (pH 7). The electrical behavior of CP is due to the low pKa values of its carboxyl groups (-COOH), which are related with the formation of carboxylate groups (-COO^-) as the pH values increase, giving rise to negative values of the ζ-potential (Trujillo-Ramírez *et al*., 2018).

When the biopolymers have charges of the same magnitude but opposite signs, the electrostatic interactions between them are strong, leading to the coacervates formation (Rousi *et al*., 2019). In the present study, API and CP biopolymers showed opposite sign ζ-potential values in the pH range from 3 to ~4. At pH values higher than 4, both API and CP biopolymers showed negative ζ-potential values, indicative of negative surface charge, being the ζ-potential values of API significantly lower than those of the CP. It has been informed that the proteins present positively charged moieties capable of interacting with negatively charged moieties of other biopolymer to form complexes at relatively low negative ζ-potential values (Hernández-Marín *et al*., 2013). From the above results, two values of pH were selected to prepare the API-CP complex coacervates: (a) 3.5, value below of the pI of API, at which opposite sign ζ-potential values were exhibited by API (+10.5 mV) and CP (-21.8 mV); and (b) 4.5, above of the pI of API, at which both biopolymers present same sign surface charge (-12.3 mV for API, and -34.7 mV for CP), but API chains still possess positive moieties capable to interact with negative moieties of CP.

3.2 *Yield, moisture, and protein content in the complex coacervates*

The yield of API-CP$_{a/b}$ decreased, and the protein content increased significantly ($p \leq 0.05$) as the API:CP weight ratio raised (Table 1). These results seem to indicate that two opposite mechanisms took place as higher API:CP weight ratios were used. By on one side, the presence of more numerous API molecules resulted in complexes richer in protein, but on the other side, the repulsive interactions between more numerous positively charged protein molecules could prevent the electrostatic attractions between CP and API molecules, which resulted in a low

Table 1. Mean values of yield, moisture, protein and hydrodynamic diameter of complex coacervates.

API-CP$_{a/b}$	Yield (%)	Moisture (%)	Protein (%)	D_h (nm)
API-CP$_{3:1/3.5}$	69.91 ± 1.10^{a}	97.97 ± 0.800^{ab}	42.50 ± 1.340^{d}	1043.0 ± 39.90^{e}
API-CP$_{5:1/3.5}$	55.06 ± 1.610^{c}	97.49 ± 0.570^{ab}	60.23 ± 2.530^{b}	1179.7 ± 26.60^{d}
API-CP$_{7:1/3.5}$	45.00 ± 1.760^{e}	97.30 ± 0.420^{b}	79.24 ± 1.890^{a}	1293.3 ± 10.80^{c}
API-CP$_{3:1/4.5}$	67.08 ± 0.690^{b}	98.89 ± 0.850^{ab}	37.91 ± 1.880^{e}	1271.7 ± 14.70^{c}
API-CP$_{5:1/4.5}$	49.73 ± 0.550^{d}	98.69 ± 0.400^{ab}	50.61 ± 0.840^{c}	2139.7 ± 10.00^{b}
API-CP$_{7:1/4.5}$	26.50 ± 0.800^{f}	98.98 ± 0.100^{a}	77.42 ± 0.830^{a}	2670.3 ± 30.90^{a}

Different superscripts in the same column indicate significant differences between the means ($p \leq 0.05$). API: amaranth protein isolate; CP: citrus pectin; D_h: hydrodynamic diameter.

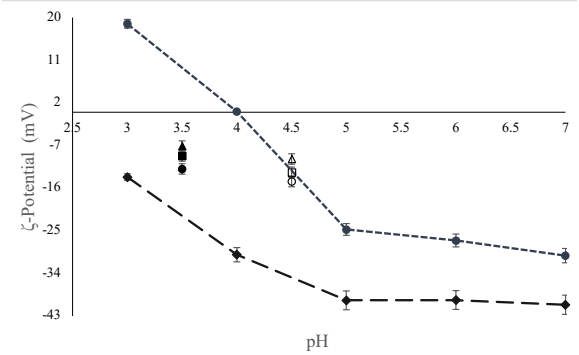

Figure 1. Variation of the ζ-potential (mV) of API (0.01 % p/p) (-•-), CP (0.01 % p/p) (-♦-) and complex coacervates API-CP$_{a/b}$. API-CP$_{3:1/3.5}$ (•), API-CP$_{5:1/3.5}$ (■), API-CP$_{7:1/3.5}$ (▲), API-CP$_{3:1/4.5}$ (o) , API-CP$_{5:1/4.5}$ (□), API-CP$_{7:1/4.5}$ (Δ) as a function of the pH.

yield of coacervates (Chang *et al*., 2016). In contrast, at relatively low API:CP weight ratios (3:1) the balance between the opposite sign charges of the API y CP at pH 3.5 favored a greater attractive association between their chains, evidenced by a higher complex coacervates yield (Chang *et al*., 2016). It would be expected that having higher concentrations of API with charges opposite to the CP would have a higher coacervate yield, though, the opposite happened. This could be due to the fact that when the pH increased from 3.4 to 4.5, the CP was charged more negatively, while the API had less positive charges, reducing the interaction between charges, which resulted in a low coacervates yield CP acquired a more negative charge, whilst API had less positive charges, reducing the interaction between the oppositely charged moieties, which resulted in a low coacervates yield (Xiong *et al*., 2020). Yield and protein content of the coacervates formed at pH 3.5 were higher than those presented by the coacervates obtained at pH 4.5 for all API:CP weight ratios (Table 1). Chang *et al*. (2016) reported a decrease in the yield of canola protein isolate and chitosan coacervates by increasing the pH of formation, due probably to the rising of the pH above the pI of the protein promoted the ionization of the amino groups limiting thus their interaction with the carboxyl groups of the polysaccharide. pH greatly influences coacervates formation by impacting more on the charge properties of proteins than polysaccharides (Xiong *et al*., 2020). Chang *et al*. (2016) mentioned that yield is one of the parameters to determine the degree of coacervation presented, whilst Rousi *et al*. (2019) mentioned that the optimal pH value should correspond to the highest yield of complex coacervate formation in each proportion of mixtures. For this study, API-CP$_{3:1/3.5}$ was the complex that presented the highest yield (69.91 ± 1.1 %) ($p \leq 0.05$).

Our results indicate that a pH of 3.5 is more favorable for obtaining coacervates from API and CP than a pH of 4.5. Thus, it is appreciated in Figure 1 that the ζ-potential values of the coacervates obtained at pH 3.5 were closer to zero (-11.97 ± 0.64, -9.24 ± 0.55, -7.14 ± 0.13 mV, for API-CP$_{3:1/3.5}$, API-CP$_{5:1/3.5}$, API-CP$_{7:1/3.5}$, respectively), than those obtained at pH 4.5 (-14.63 ± 0.31, -12.67 ± 0.45, -9.87 ± 0.14 mV, for API-CP$_{3:1/4.5}$, API-CP$_{5:1/4.5}$, API-CP$_{7:1/4.5}$, respectively). These results are in accordance agreement with the yield and protein content of de API-CP$_{a/b}$ (Table 1), indicating a more pronounced neutralization of the negative moieties of the CP at pH 3.5 by increased positive charged moieties of the API, than that occurring at pH 4.5. In addition, the formation of complex coacervates between the API and CP was evidenced by the macroscopic phase separation (Trujillo-Ramírez *et al*., 2018).

3.3 FTIR spectroscopy

FTIR spectroscopy provides insight about the molecular interactions between biopolymers. The spectra were obtained for the individual biopolymers and the complexes API-CP$_{a/b}$ (Figure 2).

CP presented spectra with a stretching absorption band of the C-O-C bond at 1012 cm^{-1} and a band at 3247 cm^{-1} corresponding to the stretching of the broad O-H bond, characteristic of this polysaccharide due to the hydrogen bonds of the galacturonic acid (Lan *et al*., 2020). At 2940 cm^{-1}, a peak associated with the C-H bond stretching of the methyl groups (-CH_3) was presented. At 1735 and 1608 cm^{-1}, stretching absorption bands of carbonyl groups (C=O) present in esterified carboxylic acid groups ($COOCH_3$) and carboxylate groups (-COO^-) were present (Raei *et al*., 2018).

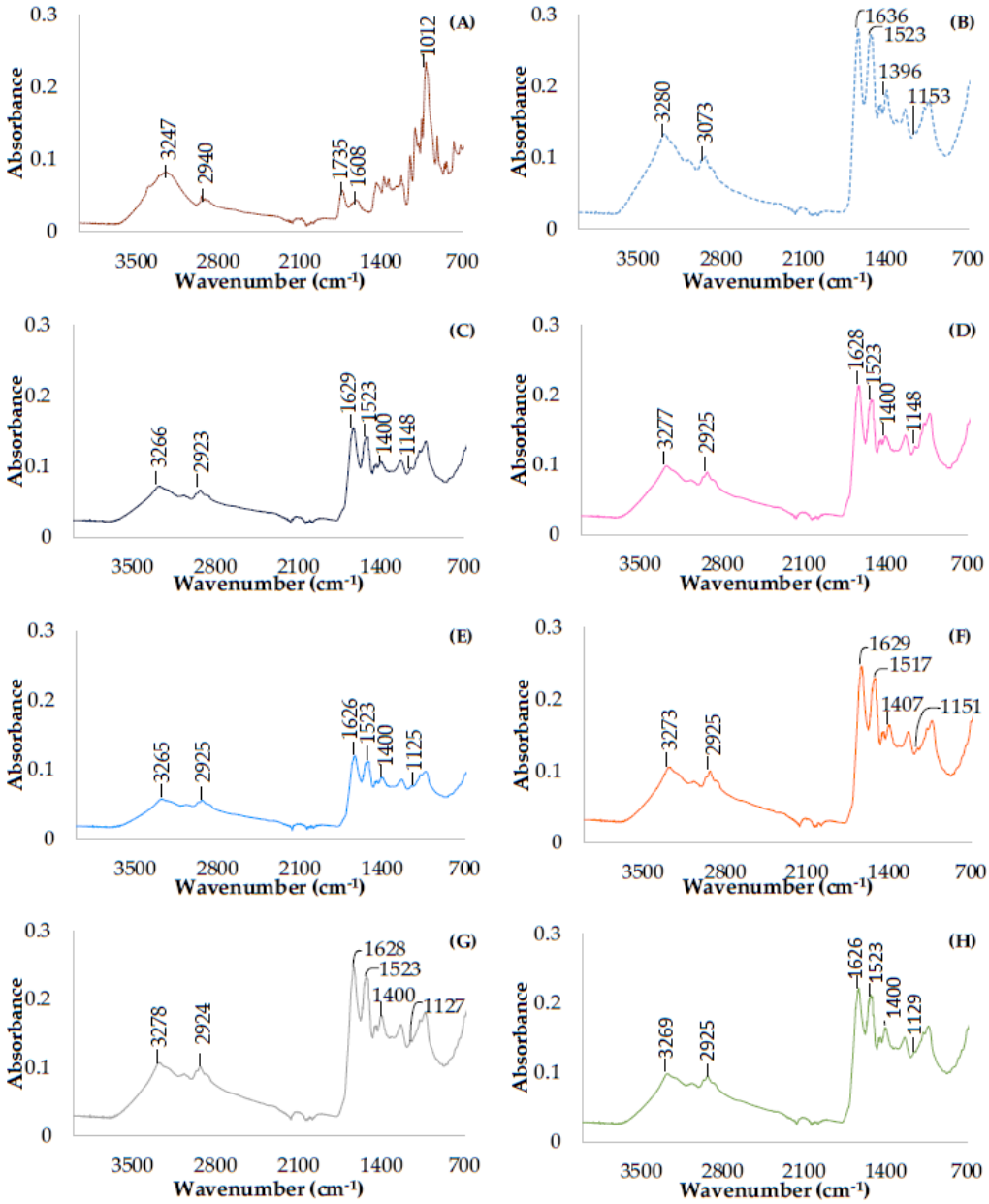

Figure 2. FTIR spectrum of amaranth protein isolate (API) (A), high methoxyl pectin (CP) (B) and complex coacervates (API-$CP_{a/b}$). API-$CP_{3:1/3.5}$ (C), API-$CP_{5:1/3.5}$ (D), API-$CP_{7:1/3.5}$ (E), API-$CP_{3:1/4.5}$ (F), API-$CP_{5:1/4.5}$ (G), API-$CP_{7:1/4.5}$ (H).

API spectrum exhibited a characteristic protein absorption band, presenting peaks at 1636, 1523, and 1396 cm^{-1} corresponding to C=O, N-H, and C-N stretching and bending bonds characteristic of amide I, II, and III, respectively. A weak band was presented at 3073 cm^{-1}, appropriate to the C-H stretching vibration, and an N-H bond strain vibration band at 3280 cm^{-1} belonging to the amine group (Rousi *et al*., 2019). These bands are like those reported for pea protein isolate (Lan *et al*., 2020) and chia protein isolate (Timilsena *et al*., 2016). It is essential to study the absorbance range from 1700 to 1600 cm^{-1}, where the amide I band is found, because the secondary structure of proteins is more susceptible to unfolding, folding or aggregation. Regarding the above, API exhibit a strong band at 1636 cm^{-1}, characteristic of β-sheet structures (Aceituno-Medina *et al*., 2013).

API-$CP_{a/b}$ spectra showed dominance by API, and differences were observed in the region considered the

fingerprint of the spectrum (1400 - 700 cm^{-1}). Peaks between 1200 and 700 cm^{-1} were exhibited, presenting a transposition of the API and CP spectra, which can be seen as a decrease at 1153 cm^{-1} (N-H, amide II) and an increase in the peak at 1396 cm^{-1} (C-N, amide III). Also, the band at 1636 cm^{-1} (C=O, amide I) decreased in all API-$CP_{a/b}$ spectra compared to that obtained for API. On the other hand, there was a decrease in the peak at 2940 cm^{-1} in all API-$CP_{a/b}$ compared to the CP spectrum. These changes suggest that the hydrogen bonds in the complex coacervates could increase because of the existence of pectin (Li *et al*., 2018), demonstrating that the coacervates formation was a consequence of the electrostatic interaction between carboxylate groups (-COO-) of CP and ammonium groups (-NH_3^+) of API (You *et al*., 2018).

3.4 Rheological properties of complex coacervates

API-$CP_{a/b}$ flow curves showed two regions, one region at low shear rates (0.001 - 0.0016 s^{-1}) known as Newtonian region, the second region of shear-thinning occurred at intermediate shear rates (0.0016 - 100 s^{-1}) (Figure 3) (Medina-Torres *et al*., 2021).

This flow behavior is typical of materials that have a structural viscosity by the formation or rearrangement of the network structure when shear is applied, exhibiting a shear-dependent behavior, this structure is recovered and reorganized when the material is at rest or in equilibrium conditions (Murillo-Martínez *et al*., 2011; Wee *et al*., 2014).

In general, API-$CP_{a/b}$ exhibited a relatively high viscosity at zero shear rate, > 1860 Pa.s (Figure 3). Making a comparison of the viscosities of the API-$CP_{a/b}$ at the same API:CP weight ratio, the viscosity decreased slightly with increasing pH. The API-$CP_{7:1/3.5}$ had the highest viscosity (17800.0 ± 923.3 Pa.s), compared to API-$CP_{7:1/4.5}$, which had the lowest viscosity (1860.0 ± 146.9 Pa.s), significantly ($p \leq 0.05$); this decrease in viscosity can be attributed to an increase in electrostatic repulsion between the biopolymers when increasing pH from 3.5 to 4.5 (Vargas *et al*., 2021).

Experimental data of apparent viscosity were fitted ($R^2 > 0.97$) to the Ellis model (Equation 2) and the values of the parameters are shown in Table 2. The viscosity at low shear rate (η_0) represents the extrapolated viscosity of solutions at zero shear rate, and it is indicative of how polymer solutions behave in the presence of entanglements and linkages (Rodrigues *et al*., 2021). The η_0 values of the API-$CP_{a/b}$ formed at a given pH, increased significantly as the API:CP weight ratio increased from 3:1 to 7:1 varying as follows: 8124.30 ± 121.40 to 36281.00 ± 127.30 Pa.s at pH 3.5, and 2004.50 ± 78.40 to 35381.00 ± 341.10 Pa.s at pH 4.5. These results seem to indicate that the presence of more numerous protein molecules available to interact with polysaccharide molecules promoted the formation of more linked and stronger coacervates networks as result of a greater interaction between charges of opposite sign of API and CP, a phenomenon more pronounced at pH 3.5. The coacervates formation is highly dependent on pH, where the complexes structure at values above or below the optimal pH is not completely structured (Liu *et al*., 2017).

Relaxation time (λ) is the time needed for a material to reorganize its structure after the constant applied stress, until it reaches a new equilibrium state, and confers critical shear rate order that evidences the final part of the Newtonian region, also shows the origin of the shear-thinning region (Hernández-Rodríguez *et al*., 2014). Many materials have a multiplicity of relaxation times, for example, polymers require much longer relaxation times because their molecular structure is more complex (Moreno, 2005). The λ values of the API-$CP_{a/b}$ followed a similar trend to those of η_0 i.e. λ values tended to increase as the API:CP weight ratio increased and pH decreased to 3.5 (701.26 ± 90.30 to 2907.20 ± 74.80 s at pH 3.5 and 368.74 ± 17.10 to 2024.20 ± 635.50 s at pH 4.5), indicative of a greater resistance of the coacervate network to flow (Rodrigues *et al*., 2021).

Table 2. Mean values of the parameters of the Ellis model of API-$CP_{a/b}$ as a function of API:CP weight ratio and pH.

API-$CP_{a/b}$	λ (s)	p	η_0 (Pa.s)
API-$CP_{3:1/3.5}$	701.26 ± 90.30^{d}	0.52 ± 0.0^{c}	8124.30 ± 121.40^{e}
API-$CP_{5:1/3.5}$	1068.50 ± 125.10^{cd}	0.53 ± 0.0^{c}	19541.00 ± 156.20^{c}
API-$CP_{7:1/3.5}$	2907.20 ± 74.80^{a}	0.55 ± 0.0^{b}	36281.00 ± 127.30^{a}
API-$CP_{3:1/4.5}$	368.74 ± 17.10^{d}	0.49 ± 0.0^{d}	2004.50 ± 78.40^{f}
API-$CP_{5:1/4.5}$	1707.50 ± 68.20^{bc}	0.59 ± 0.0^{a}	14121.00 ± 84.80^{d}
API-$CP_{7:1/4.5}$	2024.20 ± 635.50^{b}	0.60 ± 0.0^{a}	35381.00 ± 341.10^{b}

Different superscripts in the same column indicate significant differences between means ($p \leq 0.05$). η_0: viscosity at low shear rate; λ: time constant associated with the relaxation time of biopolymers in solution; p: shear thinning index. API: amaranth protein isolate; CP: citrus pectin.

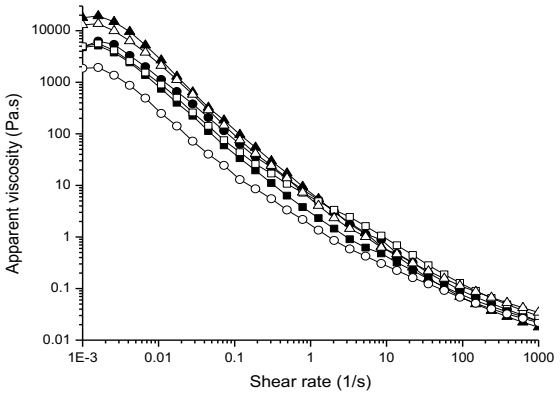

Figure 3. Flow curves of complex coacervates at different API-CP weight ratios and pH. API-$CP_{3:1/3.5}$ (•), API-$CP_{5:1/3.5}$ (■), API-$CP_{7:1/3.5}$ (▲), API-$CP_{3:1/4.5}$ (o), API-$CP_{5:1/4.5}$ (□), API-$CP_{7:1/4.5}$ (Δ).

The shear thinning index (p) represents the decrease in viscosity values with increasing shear rate (Lyklema and Olphen, 1979). The parameter p approaches a value of 1-n, where n is the flow rate of the power law model, therefore, higher p values indicate that n will have lower values, which describes a broader shear thinning behavior (Rao, 1999). In this sense, our results showed that at a constant pH, increases in the API:CP weight ratio resulted in coacervates that exhibited higher p values (0.52 ± 0.0 to 0.55 ± 74.80 at pH 3.5 and 0.49 ± 0.0 to 0.60 ± 0.0 at pH 4.5), showing that higher protein contents favored higher viscosity and drag dissipation of the coacervates, giving more pronounced shear-thinning conduct at relatively elevated shear rates (Crispín-Isidro *et al*., 2015).

For the potential implementation of coacervates in food systems as structuring agents, it is required that they present shear thinning at high shear rates, a high zero shear viscosity, in addition to an important viscoelasticity in which the elastic component (G´) prevails on the viscous one (G´´) (Hernández-Rodríguez *et al*., 2014).

The strain % of the API-$CP_{a/b}$ (Figure 4) was determined by a LVR in which G´ and G´´ presented practically constant values at low strain % values, continuing with a non-LVR value where a downward inflection of the values of the G´ and G´´ is shown to higher strain % values, corresponding to breakdown and bond reformation occurring at different rates and will depend on a more structured and interconnected network. It can be said that at a low % of deformation in the API-$CP_{a/b}$, a resistance to rupture is produced and at a higher % of deformation, a permanent deformation is produced on coacervates (Crispin-Isidro *et al*., 2015). API-$CP_{a/b}$ moduli curves were typical of weak gels showing a LVR up to a maximum strain of 0.174 % and strain thinning behavior at higher strain percentages. These oscillatory tests showed that the API:CP weight ratio and the pH influenced the viscoelastic response of the coacervates.

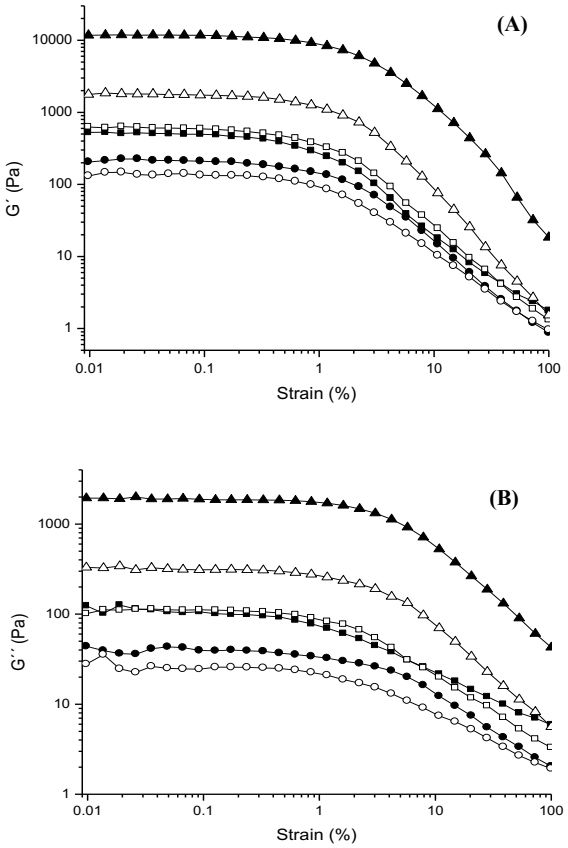

Figure 4. (A) Variation of the storage modulus (G') as a function of the strain (%) of the complex coacervates of amaranth protein isolate-citrus pectin at different ratios and pH. API-$CP_{3:1/3.5}$ (•), API-$CP_{5:1/3.5}$ (■), API-$CP_{7:1/3.5}$ (▲), API-$CP_{3:1/4.5}$ (o), API-$CP_{5:1/4.5}$ (□), API-$CP_{7:1/4.5}$ (Δ). (B) Variation of the loss modulus (G") as a function of the strain (%) of the complex coacervates of amaranth protein isolate-citrus pectin at different ratios and pH. API-$CP_{3:1/3.5}$ (•), API-$CP_{5:1/3.5}$ (■), API-$CP_{7:1/3.5}$ (▲), API-$CP_{3:1/4.5}$ (o), API-$CP_{5:1/4.5}$ (□), API-$CP_{7:1/4.5}$ (Δ).

The storage modulus (G') values in the LVR of the API-$CP_{a/b}$ increased as the API:CP weight ratio increased; thus API-$CP_{7:1/3.5}$ (11400.0 ± 354.1 Pa) and API-$CP_{7:1/4.5}$ (1690.0 ± 73.9 Pa) presented the highest G' values, followed by API-$CP_{5:1/4.5}$ (560.0 ± 35.0 Pa), API-$CP_{5:1/3.5}$ (463.0 ± 24.5 Pa), API-$CP_{3:1/3.5}$ (205.0 ± 15.1 Pa) and API-$CP_{3:1/4.5}$ (133.0 ± 18.8 Pa). High values of G' have been related with relatively strong biopolymers networks (Liu *et al*., 2017).

G´ values were higher than those of G´´ in the whole strain range studied, indicative that solid-like properties were predominant in the API-$CP_{a/b}$, i.e., elastic properties predominated over viscous properties of the API-$CP_{a/b}$. Similar behavior has been informed for complex coacervates made up of rice protein isolate-flaxseed gum (Hasanvand

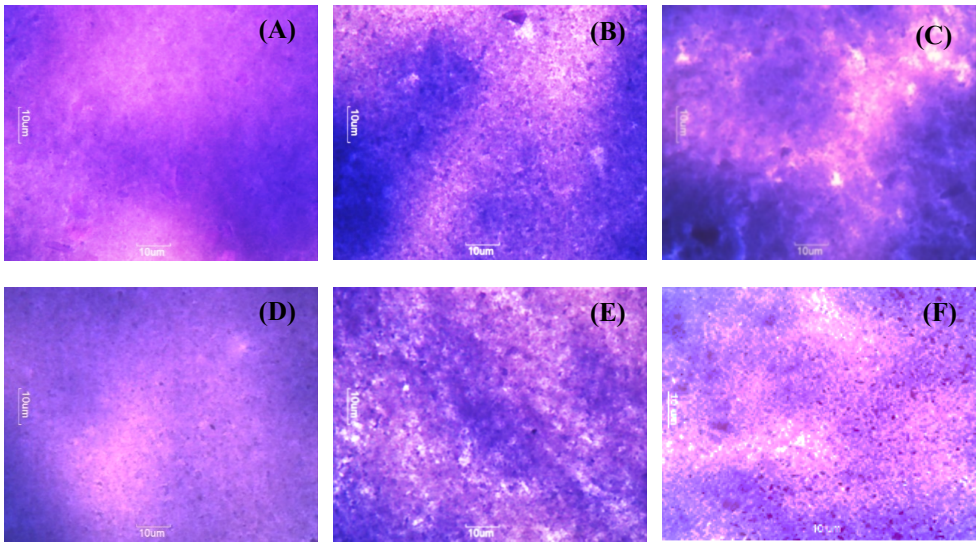

Figure 5. Optical micrographs of the complex coacervates at different ratios and different pH. API-$CP_{3:1/3.5}$ (A), API-$CP_{5:1/3.5}$ (B), API-$CP_{7:1/3.5}$ (C), API-$CP_{3:1/4.5}$ (D), API-$CP_{5:1/4.5}$ (E), API-$CP_{7:1/4.5}$ (F).

and Rafe, 2019), and canola protein isolate-gum Arabic (Stone *et al*., 2014). In contrast, coacervate complexes obtained from pea protein isolate-sodium alginate, exhibited a predominantly viscous behavior (G" > G') (Mession *et al*., 2012).

G" values in the LVR varied as follows: API-$CP_{3:1/4.5}$ (25.8 ± 3.5 Pa) < API-$CP_{3:1/3.5}$ (40.0 ± 5.8 Pa) < API-$CP_{5:1/3.5}$ (99.7 ± 7.3 Pa) < API-$CP_{5:1/4.5}$ (110.0 ± 18.1 Pa) < API-$CP_{7:1/4.5}$ (313.0 ± 35.8 Pa) < API-$CP_{7:1/3.5}$ (1860.0 ± 88.2 Pa). Our dynamic and oscillatory results indicated that relatively high API-CP weight ratio and low pH resulted in higher rheological parameters associated to a biopolymers network more structured and resistant to mechanical stress, possibly as a consequence of increases in the attractive interactions between API and CP biopolymer chains.

3.5 Particle size and microstructure of complex coacervates

The particle size of the API-$CP_{a/b}$ determined as D_h varied from 1043 ± 39.9 to 2670 ± 30.9 nm (Table 1). Both, API-CP weight ratio and pH of coacervates formation affected the D_h of the API-$CP_{a/b}$. Thus, when API-CP weight ratio was increased maintaining constant the pH formation, the D_h values of the coacervates significantly increased. By its part, higher pH value (4.5) at a constant API-CP weight ratio yielded API-$CP_{a/b}$ formed by larger particles than those formed at pH 3.5. This coacervates trend was corroborated by the optical micrographs of the API-$CP_{a/b}$ (Figure 5). Hasanvand and Rafe (2019) formed complex coacervates from rice bran protein and flaxseed gum and informed that as higher the weight ratio of biopolymers, larger the particle size of the resulting complexes. Rousi *et al*. (2019) reported similar characteristics in the coacervates formation from gelatin and gum Arabic. The increase in the particle size of the API-$CP_{a/b}$ at pH 4.5 could be due to the separation of the protein molecules with a negative charge, when interacting with the carboxylate groups of the polysaccharide, which would cause an increase in the intramolecular repulsion giving rise to less compacted particles. In the coacervates, a dissociation originated as a consequence of the progressive protonation of the carboxyl groups in the pectin structure by lowering the pH from 4.5 to 3.5 (Hasanvand *et al*. 2018). Rheological results are in agreement with a less compact structure observed for API-$CP_{a/b}$ prepared at pH 4.5 in comparison with that for the coacervates formed at pH 3.5.

Conclusions

Complex coacervates from API and CP were obtained varying the API-CP weight ratio (3:1, 5:1, and 7:1) and the pH (3.5 and 4.5) for inducing biopolymers interaction. Both, API-CP weight ratio and pH of interaction influenced the physicochemical, rheological and structural properties of the coacervates. At a given pH of interaction, as the API:CP weight ratio increased, the resulting coacervates presented higher protein content, viscoelastic and viscous parameters, and particle size. When the pH of interaction was raised from 3.5 to 4.5, the coacervates yield and the rheological properties were lower, but larger particles sizes formed which presented a relatively relaxed network structure. Thus, the coacervate that presented the highest yield (69.9 ± 1.1 %) and better-structured network exhibiting enhanced mechanical properties was that formed at pH 3.5 at a API-CP weight ratio of 7:1. All the coacervates showed structural viscosity, and exhibited shear thinning behavior

at intermediate and relatively high shear rates (0.0016 - 1000 s^{-1}). Predominance of the storage modulus (G') over the loss modulus (G") throughout the strain range studied indicated predominantly solid-like properties of the gel-like structure of the API-$CP_{a/b}$. This study could contribute to expand the knowledge about the formation of complex coacervates between pseudocereal proteins-polysaccharides, and could have applications for helping to develop gluten free bakery products, among other food products. Studies confirming or contradicting this should be carried out.

Acknowledgments

The authors thank the Consejo Nacional de Ciencia y Tecnología (CONACyT) of Mexico for financial support through grant No. 919623.

References

Aceituno-Medina, M., Lopez-Rubio, A., Mendoza, S. and Lagaron, J.M. (2013). Development of novel ultrathin structures based in amaranth (*Amaranthus hypochondriacus*) protein isolate through electrospinning. *Food Hydrocolloids 31*, 289-298. https://doi.org/10.1016/j.lwt.2015.02.025

Ach, D., Briançon, S., Dugas, V., Pelletier, J., Broze, G. and Chevalier, Y. (2015). Influence of main whey protein components on the mechanism of complex coacervation with acacia gum. *Colloids and Surfaces A: Physicochemical and Engineering Aspects 481*, 367-374. https://doi.org/10.1016/j.colsurfa.2015.06.006

Anvari, M. and Chung, D. (2016). Dynamic rheological and structural characterization of fish gelatin-Gum arabic coacervate gels cross-linked by tannic acid. *Food Hydrocolloids 60*, 516-524. http://dx.doi.org/10.1016/j.foodhyd.2016.04.028

AOAC. (1996). *Official Methods of Analysis*. Association of Official Analytical Chemist. U.S.A.

Bolontrade, A.J., Scilingo, A.A. and Añón, C.M. (2013). Amaranth proteins foaming properties: Adsorption kinetics and foam formation-Part 1. *Colloids and Surfaces B: Biointerfaces 105*, 319-327. https://doi.org/10.1016/j.colsurfb.2014.10.061

Bosnea, L.A., Moschakis, T., Nigam, P.S. and Biliaderis, C.G. (2017). Growth adaptation of probiotics in biopolymer-based coacervate structures to enhance cell viability. *LWT - Food Science and Technology 77*, 282-289. https://doi.org/10.1016/j.lwt.2016.11.056

Chang, P.G., Gupta, R., Timilsena, Y.P. and Adhikari, B. (2016). Optimisation of the complex coacervation between canola protein isolate and chitosan. *Journal of Food Engineering 191*, 58-66. http://dx.doi.org/10.1016/j.jfoodeng.2016.07.008

Chen, F.-P., Liu, L.-L. and Tang, C.-H. (2020) Spray-drying microencapsulation of curcumin nanocomplexes with soy protein isolate: Encapsulation, water dispersion, bioaccessibility and bioactivities of curcumin. *Food Hydrocolloids 105*, 105821. https://doi.org/10.1016/j.foodhyd.2020.105821

Comert, F., Malanowski, A.J., Azarikia, F., and Dubin, P.L. (2016). Coacervation and precipitation in polysaccharide-protein systems. *Soft Matter 12*, 4154-4161. https://doi.org/10.1039/C6SM00044D

Crispín-Isidro, G., Lobato-Calleros, C., Espinosa-Andrews, H., Alvarez-Ramirez, J. and Vernon-Carter, E.J. (2015). Effect of inulin and agave fructans addition on the rheological, microstructural and sensory properties of reduced-fat stirred yogurt. *LWT - Food Science and Technology 62*, 438-444. https://doi.org/10.1016/J.LWT.2014.06.042

Estrada-Girón, Y., Aguilar, J., Morales-del Rio, J., Valencia-Botin, A., Guerrero-Beltrán, J., Martínez-Preciado, A. H., Macías, E., Soltero, J., Solorza-Feria, J. and Fernández, V. (2014). Effect of moisture content and temperature, on the rheological, microstructural and thermal properties of masa (dough) from a hybrid corn (*Zea mays sp.*) variety. *Revista Mexicana de Ingeniería Química 13*(2), 429-446. http://rmiq.org/ojs311/index.php/rmiq/article/view/1335

Guo, Q., Su, J., Xie, W., Tu, X., Yuan, F., Mao, L. and Gao, Y. (2020). Curcumin-loaded pea protein isolate-high methoxyl pectin complexes induced by calcium ions: Characterization, stability and in vitro digestibility. *Food Hydrocolloids 98*, 105284. https://doi.org/10.1016/j.foodhyd.2019.105284

Hasanvand, E. and Rafe, A. (2018). Rheological and structural properties of rice bran protein-flaxseed (*Linum usitatissimum* L.) gum complex coacervates. *Food Hydrocolloids 83*, 296-307. https://doi.org/10.1016/j.foodhyd.2018.05.019

Hasanvand, E. and Rafe, A. (2019). Development of vanillin/β-cyclodexterin inclusion microcapsules using flax seed gum-rice bran protein complex coacervates. *International Journal of Biological Macromolecules 131*, 60-66. https://doi.org/10.1016/j.ijbiomac.2019.03.066

Hernández-Marín, N.Y., Lobato-Calleros, C. and Vernon-Carter, E.J. (2013). Stability and rheology of water-in-oil-in-water multiple emulsions made with protein-polysaccharide soluble complexes. *Journal*

of Food Engineering 119, 181-187. https://doi.org/10.1016/j.jfoodeng.2013.05.039

Hernández-Rodríguez, L., Lobato-Calleros, C., Pimentel-González, D.J. and Vernon-Carter, E.J. (2014). *Lactobacillus plantarum* protection by entrapment in whey protein isolate: κ-carrageenan complex coacervates. *Food Hydrocolloids 36*, 181-188. https://doi.org/10.1016/j.foodhyd.2013.09.018

Ifeduba, E.A. and Akoh, C.C. (2016). Microencapsulation of stearidonic acid soybean oil in Maillard reaction-modified complex coacervates. *Food Chemistry 199*, 524-532. https://doi.org/10.1016/j.foodchem.2015.12.011

Koupantsis, T., Pavlidou, E. and Paraskevopoulou, A. (2014). Flavour encapsulation in milk proteins - CMC coacervate-type complexes. *Food Hydrocolloids 37*, 134-142. https://doi.org/10.1016/j.foodhyd.2013.10.031

Lan, Y., Ohm, J.-B., Chen, B. and Rao, J. (2020). Phase behavior, thermodynamic and microstructure of concentrated pea protein isolate-pectin mixture: Effect of pH, biopolymer ratio and pectin charge density. *Food Hydrocolloids 101*, 105556. https://doi.org/10.1016/j.foodhyd.2019.105556

Li, Y. Zhang, X., Sun, N., Wang, Y. and Lin, S. (2018). Formation and evaluation of casein-gum arabic coacervates via pH dependent complexation using fast acidification. *International Journal of Biological Macromolecules 120*, 783-788 https://doi.org/10.1016/j.ijbiomac.2018.08.145

Liu, J., Shim, Y.Y., Shen, J., Wang, Y. and Reaney, M.J.T. (2017). Whey protein isolate and flaxseed (*Linum usitatissimum* L.) gum electrostatic coacervates: Turbidity and rheology. *Food Hydrocolloids 64*, 18-27. http://dx.doi.org/10.1016/j.foodhyd.2016.10.006

Liu, J., Shim, Y.Y., Wang, Y. and Reaney, M.J.T. (2015). Intermolecular interaction and complex coacervation between bovine serum albumin and gum from whole flaxseed (*Linum usitatissimum* L.). *Food Hydrocolloids 49*, 95-103. http://dx.doi.org/10.1016/j.foodhyd.2015.02.035

Lyklema, J. and Olphen, H.V. (1979). Terminology and Symbols in Colloid and Surface Chemistry Part 1.13. Definitions, Terminology and Symbols for Rheological Properties. *Pure and Applied Chemistry 51*(5), 1213-1218. https://doi.org/10.1351/pac197951051213

Martínez, E.N. and Añón, C. (1996). Composition and Structural Characterization of Amaranth Protein Isolates. An Electrophoretic and Calorimetric Study. *Journal of Agricultural and Food Chemistry 44*, 2523-2530.

Martínez-Velasco, A., Lobato-Calleros, C., Hernández-Rodríguez, B.E., Román-Guerrero, A., Alvarez-Ramirez, J. and Vernon-Carter, E.J. (2018). High intensity ultrasound treatment of faba bean (*Vicia faba* L.) protein: Effect on surface properties, foaming ability and structural changes. *Ultrasonics Sonochemistry 44*, 97-105. https://doi.org/10.1016/j.ultsonch.2018.02.007

Medina-Torres, N., Cuevas-Bernardino, J.C., Ayora-Talavera, T., Patrón-Vázquez, J.A., Rodríguez-Buenfil, I. and Pacheco, N. (2021). Changes in the physicochemical, rheological, biological, and sensorial properties of habanero chili pastes affected by ripening stage, natural preservative and thermal processing. *Revista Mexicana de Ingeniería Química 20*(1), 195-212. https://doi.org/10.24275/rmiq/Alim1768

Mession, J.-L., Assifaoui, A., Lafarge, C., Saurel, R. and Cayot, P. (2012). Protein aggregation induced by phase separation in a pea proteins-sodium alginate-water ternary system. *Food Hydrocolloids 28*, 333-343. https://doi.org/10.1016/j.foodhyd.2011.12.022

Monroy-Rodríguez, I., Gutiérrez-López, G.F., Hernández-Sánchez, H., López-Hernández, R. E., Cornejo-Mazón, M., Dorántes-Álvarez, L. and Alamilla-Beltrán, L. (2021). Surface roughness and textural image analysis, particle size and stability of microparticlesobtained by microfluidization of soy protein isolate aggregates suspensions. *Revista Mexicana de Ingeniería Química 20*(2), 785-805. https://doi.org/10.24275/rmiq/Alim2311

Moreno, B.R. (2005). Reología de Suspensiones Cerámicas. Editorial CSIC, Madrid.

Moschakis, T. and Biliaderis, C.G. (2017). Biopolymer-based coacervates: Structures, functionality and applications in food products. *Current Opinion in Colloid and Interface Science 28*, 96-109. https://doi.org/10.1016/j.cocis.2017.03.006

Motta, C., Castanheira, I., Gonzales, G.B., Delgado, I., Torres, D., Santos, M. and Matos, A.S. (2019). Impact of cooking methods and malting on amino acids content in amaranth, buckwheat and quinoa. *Journal of Food Composition and Analysis 76*, 58-65. https://doi.org/10.1016/j.jfca.2018.10.001

Muriel, M.J.L., Liu, J., Tan, Y., Zhou, H., Zhang, Z. and McClements, D.J. (2020). Characterization of electrostatic interactions and complex formation of γ-poly-glutamic acid (PGA) and ε-poly-*L*-lysine (PLL) in aqueous solutions. *Food Research International 128*, 108781. https://doi.org/10.1016/j.foodres.2019.108781

Murillo-Martínez, M.M., Pedroza-Islas, R., Lobato-Calleros, C., Martínez-Férez, A. and Vernon-Carter, E.J. (2011). Designing $W_1/O/W_2$ double emulsions

stabilized by protein-polysaccharide complexes for producing edible films: rheological, mechanical and water vapour properties. *Food Hydrocolloids 25*, 577-585. https://doi.org/10.1016/j.foodhyd.2010.06.015

Niu, F., Kou, M., Fan, J., Pan, W., Feng, Z.-J., Su, Y., Yang, Y. and Zhou, W. (2018). Structural characteristics and rheological properties of ovalbumin-gum arabic complex coacervates. *Food Chemistry 260*, 1-6. https://doi.org/10.1016/j.foodchem.2018.03.141

Peña-Solis, K., Soriano-Santos, J., Sánchez, C. and Díaz-Godínez, G. (2023). Functional properties and antioxidant activity of protein fractions of spirulina (*Arthrospira maxima*). *Revista Mexicana de Ingeniería Química 22*(1). https://doi.org/10.24275/rmiq/Bio2967

Raei, M., Rafe, A. and Shahidi, F. (2018). Rheological and structural characteristics of whey protein-pectin complex coacervates. *Journal of Food Engineering 228*, 25-31. https://doi.org/10.1016/j.jfoodeng.2018.02.007

Ramírez-Santiago, C., Lobato-Calleros, C., Espinosa-Andrews, H., y Vernon-Carter, E. J. (2012). Viscoelastic properties and overall sensory acceptability of reduced-fat petit-Suisse cheese made by replacing milk fat with complex coacervate. *Dairy Science & Technology 92*, 383-98. https://doi.org/10.1007/s13594-012-0077-2

Rao, M.A. (1999). *Rheology of Fluid and Semisolid Foods: Principles and Applications*. Aspen Publishers, Inc.

Rodrigues, M.Á.V., Marangon, C.A., Martins, V.C.A. and Plepis, A.M.G. (2021). Chitosan/gelatin films with jatobá resin: Control of properties by vegetal resin inclusion and degree of acetylation modification. *International Journal of Biological Macromolecules 182*, 1737-1745. https://doi.org/10.1016/j.ijbiomac.2021.05.160

Rousi, Z., Malhiac, C., Fatouros, D.G. and Paraskevopoulou, A. (2019). Complex coacervates formation between gelatin and gum Arabic with different arabinogalactan protein fraction content and their characterization. *Food Hydrocolloids 96*, 577-588. https://doi.org/10.1016/j.foodhyd.2019.06.009

Ru, Q., Wang, Y., Lee, J., Ding Y. and Huang Q. (2012). Turbidity and rheological properties of bovine serum albumin/pectin coacervates: Effect of salt concentration and initial protein/polysaccharide ratio. *Carbohydrate Polymers 88*(3), 838-846. https://doi.org/10.1016/j.carbpol.2012.01.019.

Salminen, H. and Weiss, J. (2013). Effect of pectin type on association and pH stability of whey protein-pectin complexes. *Food Biophysics 9*(1), 29-38. https://doi.org/10.1007/s11483-013-9314-3

Souza, C.J.F. and Garcia-Rojas, E.E. (2015). Effects of salt and protein concentrations on the association and dissociation of ovalbumin-pectin complexes. *Food Hydrocolloids 47*, 124-129. https://doi.org/10.1016/j.foodhyd.2015.01.010

Stone, A.K., Teymurova, A. and Nickerson, M.T. (2014). Formation and functional attributes of canola protein isolate-gum arabic electrostatic complexes. *Food Biophysics 9*(3), 203-212. https://doi.org/10.1007/s11483-014-9334-7

Timilsena, Y.P., Wang, B., Adhikari, R. and Adhikari, B. (2016). Preparation and characterization of chia seed protein isolate-chia seed gum complex coacervates. *Food Hydrocolloids 52*, 554-563. https://doi.org/10.1016/j.foodhyd.2015.07.033

Tiwari, B.K. and Singh, N. (2012). *Pulse Chemistry and Technology*. Royal Society of Chemistry. London.

Trujillo-Ramírez, D., Lobato-Calleros, C., Román-Guerrero, A., Hernández-Rodríguez, L., Alvarez-Ramirez, J. and Vernon-Carter, E.J. (2018). Complexation with whey protein hydrolysate improves cacao pods husk pectin surface active and emulsifying properties. *Reactive and Functional Polymers 123*, 61-69. https://doi.org/10.1016/j.reactfunctpolym.2017.12.011

Vargas, A.S., Delgado-Macuila, R.J., Ruiz-Espinosa, H., Rojas-Lopez, M. and Amador-Espejo, G.G. (2021). High-intensity ultrasound pretreatment influence on whey protein isolate and its use on complex coacervation with *kappa* carrageenan: Evaluation of selected functional properties. *Ultrasonics - Sonochemistry 70*, 105340. https://doi.org/10.1016/j.ultsonch.2020.105340

Ventureira, J.L., Bolontrade, A., Speroni, F., David-Briand, E., Scilingo, A.A., Ropers, M. and Anton, M. (2012). Interfacial and emulsifying properties of Amaranth (*Amaranthus hypochondriacus*) protein isolates under different conditions of pH. *LWT - Food Science and Technology 45*, 1-7. https://doi.org/10.1016/j.lwt.2011.07.024

Wee, M.S., Nurhazwani, S., Tan, K.W., Goh, K.K., Sims, I.M. and Matia-Merino, L. (2014). Complex coacervation of an arabinogalactan-protein extracted from the *Meryta sinclarii* tree (puka gum) and whey protein isolate. *Food Hydrocolloids 42*, 130-138. https://doi.org/10.1016/j.foodhyd.2014.03.005

Xiong, W., Deng, Q., Li, J., Li, B. and Zhong, Q. (2020). Ovalbumin-carboxymethylcellulose complex coacervates stabilized high internal phase emulsions: Comparison of the effects of pH and polysaccharide charge density. *Food Hydrocolloids 98*, 105282. https://doi.org/10.1016/j.foodhyd.2019.105282

You, G., Liu, X.L. and Zhao, M.M. (2018). Preparation and characterization of hsian-tsao gum and chitosan complex coacervates. *Food Hydrocolloids 74*, 255-266. https://doi.org/10.1016/j.foodhyd.2017.08.00.